Check for updates

Received: 30 April 2020 | Revised: 28 August 2020 | Accepted: 2 September 2020

DOI: 10.1002/jrs.5991

SPECIAL ISSUE - RESEARCH ARTICLE

Journal of RAMAN SPECTROSCOPY WILEY

Theoretical treatment of single-molecule scanning Raman picoscopy in strongly inhomogeneous near fields

Yao Zhang[1,2] | **Zhen-Chao Dong**[2] | **Javier Aizpurua**[1]

[1]Materials Physics Center, CSIC-UPV/EHU and Donostia International Physics Center (DIPC), Donostia-San Sebastián, 200018, Spain

[2]Hefei National Laboratory for Physical Sciences at the Microscale and Synergetic Innovation Center of Quantum Information and Quantum Physics, University of Science and Technology of China, Hefei, 230026, China

Correspondence
Javier Aizpurua, Materials Physics Center, CSIC-UPV/EHU and Donostia International Physics Center (DIPC), Donostia-San Sebastián 200018, Spain.
Email: aizpurua@ehu.es

Funding information
Eusko Jaurlaritza, Grant/Award Numbers: IT1164-19, KK-2019/00101; Ministerio de Ciencia e Innovación, Grant/Award Number: PID2019-107432GB-I00; National Natural Science Foundation of China, Grant/Award Number: 21804125

Abstract

Tip-enhanced Raman spectroscopy (TERS) of a single molecule is commonly described by considering the change in the polarizability of the molecule with respect to a normal coordinate induced by homogeneous illumination. However, the local fields induced by nanoscale and atomic-scale features at the surface of metallic clusters and nanogaps show strong inhomogeneities in their spatial distribution, which induces breaking of Raman selection rules. In this context, the spatial extension of the molecular electronic states subjected to strongly varying local fields challenges the validity of the point–dipole approximation as an adequate description of TERS in such configurations. Here, we introduce a general treatment to simulate single-molecule TERS spectra and their energy-filtered vibrational fingerprints maps, in which the polarization properties of the single molecule and that of the optical enhancing nanoresonator can be calculated separately and then conveniently combined to obtain the total Raman cross section of the molecule under the strongly inhomogeneous field. We apply the general method to study tip-enhanced scanning Raman picoscopy of a 4,4′-bipyridine and biphenyl molecules in the proximity of a silver icosahedral cluster with a few atoms at the tip apex mimicking an enhancing picocavity. The polarization of the molecules is calculated within density functional theory (DFT), and the optical response of the tip is calculated within a classical atomistic discrete–dipole approximation. The Raman spectra are found to be extremely sensitive to the spatial distribution of the local fields and to the orientation of the molecule. Our calculations show that the spatial mapping of molecular vibrational fingerprints, as probed by a tip with atomic protrusions, is capable to reveal intramolecular features of a single molecule in real space and thus establish a robust basis for scanning Raman picoscopy.

KEYWORDS

nanoantena, picocavity, plasmonics, scanning Raman picoscopy, surface-enhanced Raman spectroscopy, tip-enhanced Raman spectroscopy

Additional supporting information related to the detailed derivation of the molecular polarizability expressed in terms of the atomic contributions and the vibrational modes of the biphenyl molecule with their corresponding electric field distributions may be found online in the Supporting Information section at the end of this article.

This is an open access article under the terms of the Creative Commons Attribution-NonCommercial License, which permits use, distribution and reproduction in any medium, provided the original work is properly cited and is not used for commercial purposes.
© 2020 The Authors. Journal of Raman Spectroscopy published by John Wiley & Sons Ltd

1 | INTRODUCTION

Since the concept of tip-enhanced Raman spectroscopy (TERS) was first proposed in 1985[1] and experimentally demonstrated in 2000,[2-5] this technique has become a powerful tool to obtain chemical identification of molecular species in the nanoscale, showing both high spectral sensitivity and exquisite spatial resolution when combined with scanning tunneling microscopy (STM) or atomic forced microscopy (AFM),[6-13] particularly when operated at ultrahigh-vacuum and low-temperature conditions.[14-16] These unique properties are originated from the nanometric localization and enhancement of local electromagnetic fields at the apex of a metallic probing tip, which often forms a cavity between the metallic tip and the substrate, leading to the excitation of localized surface plasmons (LSPs).[17] A target molecule or molecular layer located beneath the tip or inside the cavity experiences the enhancement of the local field both from the incoming radiation, as well as from the outgoing radiation; thus, the enhancement of the Raman signal is found to scale with the fourth power of the local field enhancement.[18-20] This electromagnetic field enhancement can be intensified or decreased due to other effects connected with chemical polarizations of the molecule-substrate system[21] or optomechanical feedback mechanisms,[22-25] which have been recently explored as additional enhancing mechanism of molecular Raman scattering in plasmonic cavities.

The Raman signal is extremely sensitive to the spatial distribution of local fields induced by the incoming light that probes the molecules; therefore, it turns to be of paramount importance to develop an accurate quantitative estimation of the optical near-field response in specific TERS configurations. A variety of theoretical methods including classical and quantum approaches have been adopted to estimate the local field and the corresponding Raman signal enhancement.[26-28] Both classical and quantum methods often adopt a smooth and continuous description of metallic interfaces and molecular objects to obtain the distribution of local fields based on the solution of Maxwell's equations or of the Schrödinger equation, respectively. Among the classical methods to obtain local fields, the finite-element method (FEM),[29,30] the finite-difference in time-domain (FDTD) method,[31,32] and the boundary element method (BEM),[33-36] among others, have been commonly applied to metallic nanoantenas and tips. In all of these methods, the local field properties are usually determined by the smooth boundaries of a nanoscale morphology of the nanostructure (tip or tip-substrate cavity) with a more or less sophisticated description of the roughness. Even in quantum descriptions of the optical response of metallic cavities, a jellium model[37-41] of the electron gas, which relies on a smooth description of the electronic density at the metal-vacuum interface, is often considered as a valid approach to obtain the optical polarization of metallic nanoresonators within the use of the time-dependent density functional theory (TDDFT). Beyond these continuous approaches, atomistic models that refer the optical response of matter to its atomic constituents provide a roadmap to reveal the role of subnanometric features in metallic cavities and tips that introduce significant differences in the local field distributions around the nanoresonators (tips and/or gaps) and thus on its action onto the molecules deposited nearby.[42-45]

Recent studies have shown the ability of TERS to achieve submolecular resolution in the Raman signal of different vibrational fingerprints of a single molecule at low temperature and ultrahigh vacuum[16] and even identify two different adjacent molecules.[46] The spatial resolution of single-molecule TERS has now reached the Ångström level, driven by the development of the scanning Raman picoscopy (SRP) technique,[47,48] which relies on the exquisite control of the localization of near fields at a few atoms on the apex of the metallic scanning tips, the so-called picoresonator or picocavity, capable to resolve the vibrations of a single chemical bond. Remarkably, this extreme level of field localization does not only occur at the apex of a tip in scanning probe microscopy configurations but is also present in standard surface-enhanced Raman spectroscopy (SERS) of molecules located in narrow gaps.[49] Atomic-scale protrusions in such plasmonic gaps are also capable of producing picocavities that localize the induced near fields to the atomic scale and thus probe single bonds of molecules and induce breaking of Raman selection rules.[25,50,51]

In order to address this extreme localization of light, it is necessary to implement a methodology that considers the atomistic nature of both the metallic nanocluster and the single molecule in order to account for the strong inhomogeneity of the near-field distribution in the description of the Raman signal. Recently, Barbry et al. proposed a full quantum atomistic calculation of the plasmonic response of a metallic cavity based on TDDFT,[28] which showed the possibility of localization of plasmonic local fields below 1 nm^3 at atomic-scale vertices and edges, similar to those existing in scanning tips. Interestingly, it has been shown that these atomic-scale features of the plasmonic response can be reasonably well reproduced with the use of a "classical" atomistic approach that follows the quantum mechanical electron density profile of the surface atoms,[52] thus validating the optical near-field response obtained for metallic clusters and nanoparticles by other classical studies

such as those based on the discrete–dipole approximation (DDA).[43-45]

A single molecule positioned in a plasmonic field localized at the atomistic scale shows a behavior of the polarization totally different from that of a molecule located in an homogeneous field. If the spatial distribution of the local field is comparable or even smaller than the size of the probed molecule, the different atoms within the molecule will be subjected to different local field amplitudes and directions, resulting in the breakdown of Raman-active criteria and selection rules based on molecular symmetries.[53] Different strategies have been adopted to describe the influence of local fields on the polarization of a molecule, which include evaluating the integrals between the molecular wavefunctions and the local field amplitudes to describe the Raman interaction. In this context, we can cite for instance the Gaussian-type field representation[54] or the locally integrated Raman polarizability density method.[45] However, these methods often require a complete calculation whenever the molecular system or its relative configuration within the cavity is modified, jeopardizing the possibility of obtaining massive Raman maps of molecular systems with generality.

Here, we introduce a simplified general treatment of single-molecule Raman scattering in the presence of a general nanoresonator that localizes light, including the extreme case of localization induced by a picoresonator. Within this treatment, the optical response of the nanostructure is first calculated by standard classical electromagnetic simulation methods (e.g., FEM, BEM, or TDTD), and the polarization of the single molecule is calculated with the use of quantum chemistry packages (e.g., Gaussian, VASP, or QChem). We first calculate the Greens function and local electric field of the nanoresonator of choice, considering the particular incident illumination used in the Raman scattering process. The molecular polarizability derivatives are calculated from the atomic contributions of the molecule in order to compose the Raman dipole moment, and from the total Raman dipole, one can obtain the Raman scattering cross section. The Raman spectra are then obtained by summing up the contribution from all the vibrational modes. As an example of the procedure, here we adopt a fully atomistic model to describe both the optical response of a metallic probing tip and that of the Raman dipole moment of the molecule. This approach allows for exposing the effect of atomic-scale features and interactions through the output of the Raman signal, revealing extreme spectral and spatial dependencies of the vibrational fingerprints on these features. The tip is described as an Ag_{1415} nanocluster with the use of an atomistic DDA method to reproduce the strongly inhomogeneous fields around the atoms of the tip apex. Two different single molecules (4,4′-bipyridine [44BPY] and biphenyl) are considered, and their chemical composition is described at a quantum atomistic level within DFT. The molecules are located under the strongly inhomogeneous local fields of the silver apex with specific realisitic orientations. The Raman signal of the single molecules can be retrieved from the full atomistic calculation that considers the inhomogenous illumination induced by the local fields of the silver apex. We analyze the Raman spectra for different molecular orientations and simulate the real-space energy-filtered Raman maps of single molecules and molecular dimers as obtained by theoretically scanning the tip over the molecules. This treatment of Raman scattering for single molecules near a picocavity can be generalized to any molecule and any nanostructure shape as it relies on the separate calculation of their optical properties independently. Such a general procedure can enable systematic and massive calculation of experimental Raman images of a variety of molecules as obtained with SRP and thus allows for interpretation of single-molecule Raman scattering at intramolecular level.

2 | THEORETICAL TREATMENT

We introduce here the general theoretical treatment to address the Raman scattering cross section, $d\sigma_k^{\mathrm{Raman}}/d\Omega$, under inhomogeneous illumination in a system composed by a generic nanoresonator and a molecule. The flow chart of the overall simulation procedure is shown in Figure 1. In short, the optical response of the nanoresonator can be calculated by any method of electromagnetism, from which we can obtain the two-point Green's function $\overleftrightarrow{\mathrm{G}}(\mathbf{r},\mathbf{r}')$ of the system relating positions $\mathbf{r}$ and $\mathbf{r}'$ as well as the local electric field $\mathbf{E}^{\mathrm{loc}}(\mathbf{r})$ induced by the external illumination at position $\mathbf{r}$. The optical properties of the molecule can be obtained from a variety of methods of quantum chemistry, from which the derivatives of the atomistic molecular polarizability, $\partial\alpha^{\mathrm{mol}}/\partial\xi_n$, corresponding to each atomic coordinate ξ_n of atom n can be obtained. These two separated calculations can then be combined to provide the atomistic Raman dipole contribution of each atom n to the total Raman dipole moment p_k^{Raman}. The emission of the Raman dipole moment corresponding to a given kth vibrational mode of the molecule, scattered out by the nanoresonator to the far field, can be described through the corresponding Green's function, $\overleftrightarrow{G}_k(\mathbf{r}_\infty,\mathbf{r}_\mathrm{n})$. The total Raman spectrum can be obtained by adding up the contribution from all the vibrational peaks. The details of this model will be explained in the following sections.

2.1 | Atomistic classical electrodynamical calculation of the probe local near field

We first focus on the optical response of a metallic nanoparticle as a probing nanoresonator that produces the local distribution of near fields. We consider a classical atomistic approach to calculate the nanoresonator's response, but any other method that properly accounts for the atomic-scale features at the surface of the nanoresonator is equally valid. In this atomistic description, the plasmonic response of the nanoresonator can be related to the polarization of each constituent atom, including the dipole–dipole interactions between the different atomic dipoles. This method is the so-called DDA.[55] The atomistic polarizability of each ith atom, α_i, depends on the particular material, and the electromagentic interaction between two atoms is estimated from their point–dipole interaction for simplicity. The polarized atomic dipole moment at each ith atom of the nanoresonator, $\mathbf{p}_i$, induced by the electric field acting on the atom, $\mathbf{E}_i$, can be expressed as $\mathbf{p}_i = \alpha_i \mathbf{E}_i$. The electric field that each atom experiences not only contains the incident electric field $\mathbf{E}_i^{\text{inc}}$ but also includes the field produced by the other atomic dipole moments as

$$\mathbf{E}_i = \mathbf{E}_i^{\text{inc}} - \sum_{j \neq i} \mathbf{A}_{ij} \mathbf{p}_j = \alpha_i^{-1} \mathbf{p}_i, \tag{1}$$

where $\mathbf{A}_{ij} = -\left(3\hat{\mathbf{r}}_{ij}\hat{\mathbf{r}}_{ij} - \mathbf{I}\right)/r_{ij}^3$ denotes the dipole–dipole interaction between atoms i and j and r_{ij} is the distance between those atoms, with the direction of the distance denoted by the unit vector $\hat{\mathbf{r}}_{ij}$. We define the diagonal term $\mathbf{A}_{ii} = \alpha_i^{-1}$, and the above equation can be written as a linear set of equation for each ith atom of the total number of atoms of the nanoresonator, N, as

$$\sum_{j=1}^{N} \mathbf{A}_{ij} \cdot \mathbf{p}_j = \mathbf{E}_i^{\text{inc}}. \tag{2}$$

Equation (2) can be solved numerically to obtain the self-consistent atomistic polarizations, $\mathbf{p}_i$, and hence, the absorption cross section, σ_{abs}, of the nanoresonator can be expressed in terms of these induced atomistic dipole moments as

$$\sigma_{abs} = \frac{4\pi\omega}{c} \text{Im}\left\{ \sum_{i=1}^{N} \mathbf{p}_i \cdot \mathbf{E}^{\text{inc}} \right\} / \left|\mathbf{E}^{\text{inc}}\right|^2, \tag{3}$$

where Im{} is the imaginary part of {}, N is the total number of atoms in the nanoresonator, ω is the frequency of the incident field, and c is the speed of light.

The local electric field, $\mathbf{E}^{\text{loc}}(\mathbf{r})$, induced at a generic position $\mathbf{r}$ can be estimated from the sum-up of the atomistic dipole contributions as

$$\mathbf{E}^{\text{loc}}(\mathbf{r}) = \sum_{i=1}^{N} \left(\frac{3[\mathbf{p}_i \cdot (\mathbf{r} - \mathbf{r}_i)](\mathbf{r} - \mathbf{r}_i)}{|\mathbf{r} - \mathbf{r}_i|^5} - \frac{\mathbf{p}_i}{|\mathbf{r} - \mathbf{r}_i|^3} \right), \tag{4}$$

where $\mathbf{r}_i$ is the position of each atom in the nanoresonator. The value of $\mathbf{E}^{\text{loc}}$ is one of the key ingredients

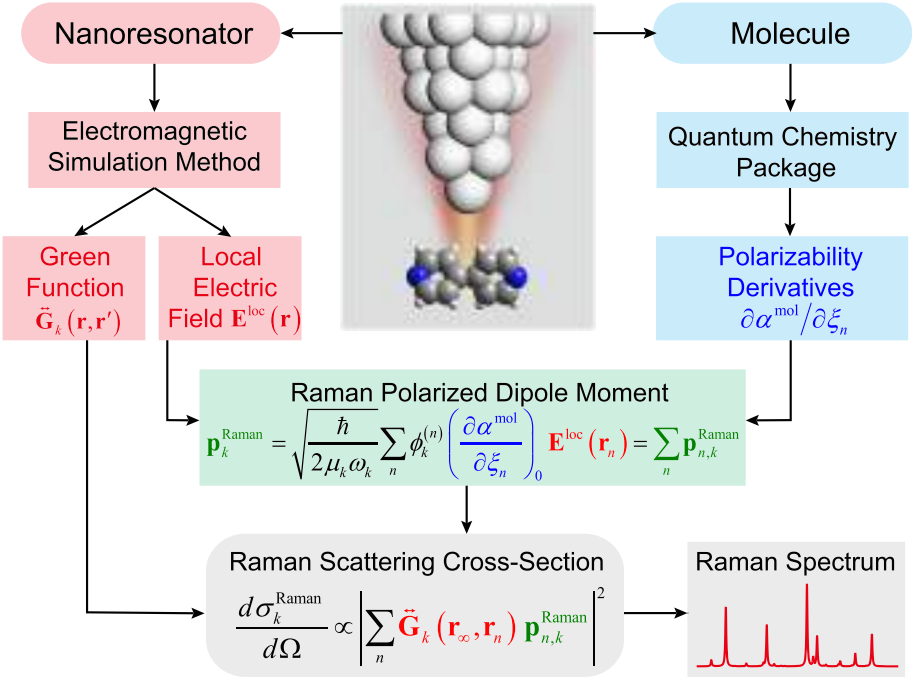

FIGURE 1 Flow chart for the procedure for simulation of single-molecule Raman scattering. See the text for an explanation of the magnitudes calculated within each step of the approach

to calculate the Raman cross section of a molecular fingerprint located in the vicinity of the nanoresonator, as observed in the flow chart of the procedure in Figure 1.

2.2 | Calculation of the molecular atomistic Raman polarizabilities within DFT

In order to account for the inhomogeneity of the local near fields acting on the different atoms of a molecule, we will express the total Raman dipole of a molecule in terms of the atomistic Raman polarizabilities. We first consider the induced dipole moment of a single molecule, $\mathbf{p}^{\mathrm{ind}}$, polarized by an incident electric field, which can be written as

$$\mathbf{p}^{\mathrm{ind}} = \alpha^{\mathrm{mol}}\mathbf{E}^{\mathrm{inc}} = \alpha_0^{\mathrm{mol}}\mathbf{E}^{\mathrm{inc}} + \sum_k \left(\frac{\partial \alpha^{\mathrm{mol}}}{\partial Q_k}\right)_0 Q_k \mathbf{E}^{\mathrm{inc}} + o\left(Q_k^2\right), \tag{5}$$

where α^{mol} is the polarizability of the single molecule, $\mathbf{E}^{\mathrm{inc}}$ is the incident electric field, and Q_k is the normal coordinate of the kth vibrational mode. The second term of Equation (5) corresponds to the Raman scattering process, from which we can define the Raman dipole moment, $\mathbf{p}_k^{\mathrm{Raman}}$, and the Raman polarizability, $\alpha_k^{\mathrm{Raman}}$, as

$$\mathbf{p}_k^{\mathrm{Raman}} = \left(\frac{\partial \alpha^{\mathrm{mol}}}{\partial Q_k}\right)_0 Q_k \mathbf{E}^{\mathrm{inc}} \equiv \alpha_k^{\mathrm{Raman}}\mathbf{E}^{\mathrm{inc}}. \tag{6}$$

The detailed description of the derivation of the molecular polarizability expressed in terms of the atomic contributions can be found in the Supplementary Information. In brief, the Raman polarizability, usually expressed in terms of normal coordinates Q_k, can be referred to the atomic coordinates $\xi^{(n)}$ of each atom n of the molecule, by applying a coordinate transformation. Hence, one can express the Raman polarizability as

$$\alpha_k^{\mathrm{Raman}} = \left(\frac{\partial \alpha^{\mathrm{mol}}}{\partial Q_k}\right)_0 Q_k = \sqrt{\frac{\hbar}{2\mu_k\omega_k}} \sum_{n=1}^{M} \phi_k^{(n)} \left(\frac{\partial \alpha^{\mathrm{mol}}}{\partial \xi^{(n)}}\right)_0 \equiv \sum_{n=1}^{M} \alpha_k^{(n)} \tag{7}$$

with M the number of the atoms in the molecule, μ_k and ω_k the reduced mass and wavenumber of the kth vibrational mode, $\phi_k^{(n)}$ the normalized displacement of the nth atom corresponding to the kth vibrational mode, and $\xi^{(n)}$ the coordinate of the nth atom. From Equation (7), we define $\alpha_k^{(n)}$ as the atomistic Raman polarizability of the nth atom corresponding to the kth vibrational mode. Under this transformation, we can understand the Raman polarizability of a molecule as a result of the contributions of the Raman polarization of each atom, $\alpha_k^{(n)}$. The atomistic Raman dipole moment of the nth atom in the molecule for the kth vibrational mode, $\mathbf{p}_{n,k}$, induced by an incident electric field $\mathbf{E}^{\mathrm{inc}}$, can thus be written as

$$\mathbf{p}_{n,k}^{\mathrm{Raman}} = \alpha_k^{(n)}\mathbf{E}^{\mathrm{inc}}. \tag{8}$$

In order to obtain the derivative of the polarizability corresponding to each atomic coordinate, as well as the reduced mass μ_k, vibrational wavenumber ω_k, and normalized displacement $\phi_k^{(n)}$ to be used in Equation (7), we can adopt any reasonable scheme within molecular quantum chemistry calculations. In particular, we use here the DFT package implemented in the Gaussian09 software[56] with the hybrid functional B3LYP and the 6-31G(d) basis set to calculate all the relevant vibrational parameters and hence obtain the atomistic full Raman polarizability tensor of each atom of the molecules under study.

2.3 | Calculation of inhomogeneous field-enhanced Raman scattering

In this section, we outline the methodological approach that allows for calculating the Raman cross section of a molecule subjected to a strongly inhomogeneous field. If the single molecule is located in an inhomogeneous local electric field, the atomistic Raman dipole moment of the nth atom of the molecule for the kth vibrational mode induced by the local electric field $\mathbf{E}^{\mathrm{loc}}(\mathbf{r}_n)$ can be defined as

$$\mathbf{p}_{n,k}^{\mathrm{Raman}} = \alpha_k^{(n)}\mathbf{E}^{\mathrm{loc}}(\mathbf{r}_n). \tag{9}$$

The local field induced by the nanoresonator on each atom of the molecule, $\mathbf{E}^{\mathrm{loc}}(\mathbf{r}_n)$, can be obtained from the solution of Equation (4), which, within the atomistic description presented in this section, can be written as

$$\mathbf{E}^{\mathrm{loc}}(\mathbf{r}_n) = \sum_{i=1}^{N} \overleftrightarrow{\mathrm{G}}(\mathbf{r}_n, \mathbf{r}_i)\, \mathbf{p}_i = \sum_{i=1}^{N} \overleftrightarrow{\mathrm{G}}_{ni} \sum_{j=1}^{N} \mathbf{A}_{ij}^{-1}\mathbf{E}_j^{\mathrm{inc}}(\omega), \tag{10}$$

where $\overleftrightarrow{\mathrm{G}}(\mathbf{r}_n, \mathbf{r}_i) \equiv \overleftrightarrow{\mathrm{G}}_{ni}$ is the Green's function for the dipole moment $\mathbf{p}_i$ and ω is the frequency of incident light. The value of $\mathbf{E}^{\mathrm{loc}}(\mathbf{r}_n)$ could be derived from any other method to solve Maxwell's equation, as far as the atomistic features on the surfaces of the nanoresonator are properly described in the boundary conditions.[52]

The action of the local field on each atom n allows for determining the atomistic Raman polarizabilities folllowing Equation (9). Hence, the field produced by the contribution from all the atomistic Raman dipoles of the molecule at an arbitrary position $\mathbf{r}$ can be expressed as

$$\mathbf{E}^{\mathrm{mol}}(\mathbf{r}) = \sum_{n=1}^{M} \overleftrightarrow{\mathrm{G}}_k(\mathbf{r},\mathbf{r}_n)\mathbf{p}_{n,k}^{\mathrm{Raman}}, \tag{11}$$

where $\overleftrightarrow{\mathrm{G}}_k(\mathbf{r},\mathbf{r}_n)$ is the Green's function for the atomistic Raman dipole moment $\mathbf{p}_{n,k}^{\mathrm{Raman}}$ with radiation frequency $(\omega - \omega_k)$. In particular, the far-field radiation of the polarized molecule, $\mathbf{E}_{\mathrm{far}}^{\mathrm{mol}}(\mathbf{r}_\infty)$, can be also expressed as a sum of the contributions from each atom in the molecule:

$$\mathbf{E}_{\mathrm{far}}^{\mathrm{mol}}(\mathbf{r}_\infty) = \sum_{n=1}^{M} \overleftrightarrow{\mathrm{G}}_k(\mathbf{r}_\infty,\mathbf{r}_n)\mathbf{p}_{n,k}^{\mathrm{Raman}}, \tag{12}$$

which allows for determining the Raman scattering cross section as

$$\frac{d\sigma_k^{\mathrm{Raman}}}{d\Omega} \propto \left| \sum_{n=1}^{M} \overleftrightarrow{\mathrm{G}}_k(\mathbf{r}_\infty,\mathbf{r}_n)\mathbf{p}_{n,k}^{\mathrm{Raman}} \right|^2. \tag{13}$$

In this expression, the nanoantenna effect induced by the nanocluster is twofold. On the one hand, the far-field Green's function in Equation (13) provides an enhancement of the radiation of the molecular dipole. On the other hand, the atomistic Raman dipole moment is also enhanced by the local field according to Equation (9). Both contributions provide the well-known $|\mathbf{E}^{\mathrm{loc}}|^4$ dependence on the local field of the final Raman intensity. In the following section, we will show the results of this method when applied to calculate the Raman scattering of a molecule enhanced by a silver cluster as a probing tip.

3 | SCANNING RAMAN PICOSCOPY OF A SINGLE MOLECULE

We show now the application of the method described above to calculate the Raman spectrum of an exemplary molecule in the strongly inhomogeneous field of a picocavity produced by the few atoms in a metallic cluster. The Raman signal of such a system allows for performing SRP, as shown below. We first provide the details of the optical response of both picoscale resonator and molecule to later address its Raman scattering spectrum and picoscopy.

3.1 | Plasmonic response of a picocavity: A silver nanocluster

We first consider the typical configuration of a picoscale resonator composed of a few protruding atoms in an Ag cluster. This type of configuration is similar to the one often found in scanning probe microscopy tips, for instance. As pointed out in the methodological section, any methodology to solve Maxwell's equations in such an atomic-scale system could be used to provide the solution of the far-field and near-field response of the cluster. Here, we choose the classical DDA to put the emphasis on the atomistic aspects of the field localization. The cluster configuration is built up from a regular icosahedron with 1415 silver atoms, where each atom is regarded as a sphere with an atomic radius $r = 1.598$ Å, and a crystal lattice constant ($a = 4.0897$ Å). The corresponding atomic polarizability, shown in the inset of Figure 2b, is deduced from the Clausius–Mossotti relationship with the experimental optical parameters of silver.[57] Figure 2b shows a typical absorption spectrum for this nanocluster, as calculated from DDA calculations following the procedure described in the methodological section. A resonant peak can be observed at 3.47 eV when the electric field of an incident planewave is polarized along the z-axis (see axis in Figure 2a). The corresponding local electric field distributions are shown in Figure 2c–h for different energies and evaluation planes. If the frequency of the incident electric field is far from the resonant peak (off-resonant condition, for instance at $\omega = 2.0$ eV), the local electric field in the yz-plane (cluster side cross section as shown in Figure 2c) exhibits a general dipolar feature with clearly visible field enhancement close to the apex of the nanocluster, as "hot-spots." The spatial confinement of these hot-spots is at the atomic scale, clearly confined to the last atom or pair of atoms in the apex of the cluster. This effect has been identified in the literature as a lightning rod effect at the atomic scale, produced by the "curvature" of the atomic protrusions,[52] an effect validated by atomistic ab-initio TDDFT calculations of such cluster's response.[28,58] This ultra-confined local field can be observed more clearly from the field distribution in the xy-plane (cross section below the nanocluster apex) at different distances from the apex. For the closest evaluation distance ($d = 0$ nm denotes a xy-plane tangent to the surface of the apex atom), the lateral extension of the hot-spot is smaller than 1 nm (see Figure 2d), whereas for a xy-plane more distant from the apex atom ($d = 0.5$ nm), the field distribution is more spread (see Figure 2e). Under resonant incidence ($\omega = 3.47$ eV), the atomic-scale hot-spots are much more localized, as illustrated in Figure 2f–h. Even for a xy-plane under the atomistic tip as far as 0.5 nm away (Figure 2h), the local electric field

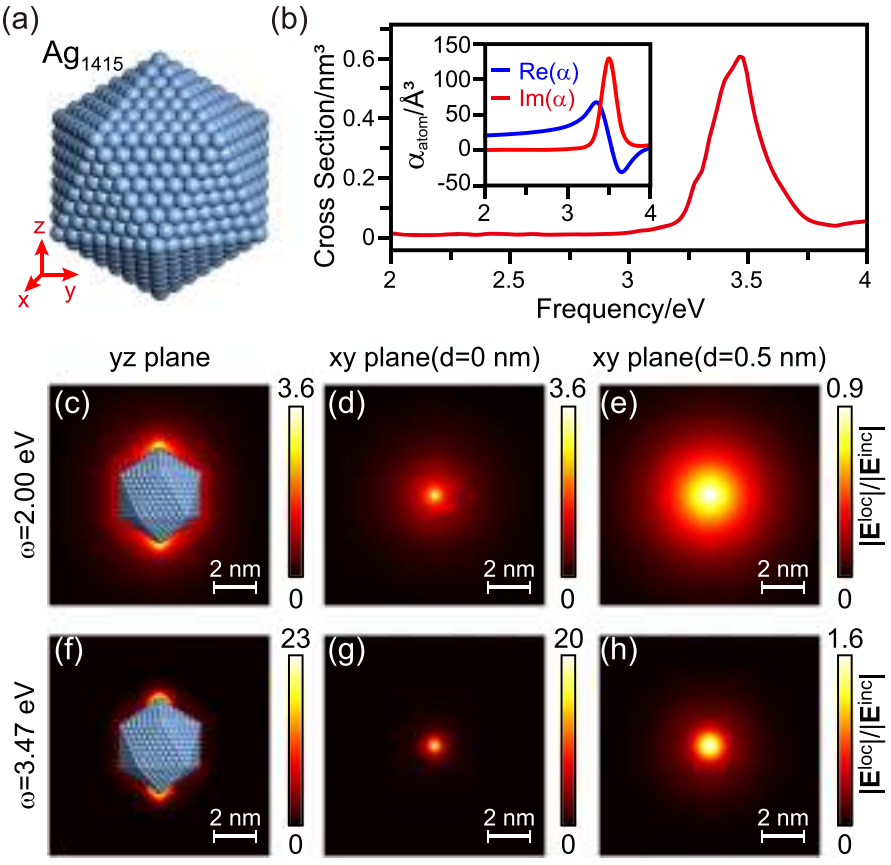

FIGURE 2 (a) Atomistic structure of a Ag_{1415} nanocluster with a regular icosahedron structure. The orientation is referred to the axis displayed on the bottom-left corner. (b) Absorption spectrum of the nanocluster in (a) for an incident planewave with electric field polarized along the z-axis, E_z. The inset shows the real and imaginary part of the atomic polarizability of the Ag atoms forming the nanoscluster. (c–e) Induced local electric field distribution in the proximity of the nanocluster for an incident optical planewave with off-resonance energy ($\omega = 2.00$ eV) in the (c) yz-plane, in the (d) xy-plane at a distance of $d = 0$ nm, and in the (e) xy-plane at a distance $d = 0.5$ nm from the apex of the nanocluster. (f)–(h) show the same local field distributions as in (c)–(e), for incident light in resonance with the nanocluster dipolar mode ($\omega = 3.47$ eV)

is still confined in a subnanometer region. The inhomogeneity and strong localization of the local fields as those found here are thus excellent candidates to set atomic-scale light sources enabling SRP,[16,46,48,59-61] as well as other atomically resolved molecular spectroscopies, such as fluorescence.[62]

3.2 | Raman response of molecules: 4,4′-BPY and biphenyl

As shown in the methodological section, the treatment of the Raman polarizability of the molecules is a key ingredient in the calculation of the Raman scattering cross section. We consider here the 4,4′-BPY and biphenyl molecules to show the application of the methodology. Their chemical structures are shown in Figure 3a, where both molecules exhibit a similar double-ring geometry, except for the replacement of the 4- and 4′-sites by N atoms, in the 4,4′-BPY molecule. For homogeneous illumination, the Raman polarizability for a particular vibrational mode can be retrieved from the derivative of the molecular polarizability, as directly obtained from DFT calculations. The results of the Raman spectra for both molecules show very similar features, as shown in Figure 3b, because of the similar molecular structure. Three main peaks are dominant, and labeled as ν_{12}, Ω and ν_{8a} modes, following the Varsányi's symbols.[63,64] Figure 3c shows the schematics of the vibrational motion corresponding to these three vibrational modes for the 4,4′-BPY molecule.

We show now the main differences in the Raman polarization of the three relevant modes when the molecules are inhomogenously illuminated. To that end, we first obtain the atomistic Raman dipole of each atom in the molecule, induced by the particular distribution of the illumination, following Equation (9), and hence, calculate the corresponding electric field produced by the Raman polarized molecule, as given by Equation (4), but with the atomistic dipole $\mathbf{p}_i$ replaced by the atomistic Raman dipole of each n atom, $\mathbf{p}_{n,k}^{\text{Raman}}$, for each kth mode. We first apply this procedure to the case of homogeneous illumination. The induced field intensities $|\mathbf{E}^{\text{mol}}|$ from the polarized molecule, as obtained from Equation (11), are calculated for the three relevant modes for an incident electric field polarized along the z-direction, exhibiting the relationship between the atomic vibrations and electric field distributions for each of them. The fields are calculated on the two pyridine ring planes of the 44BPY molecule rather than on the xy-plane. The field distributions in Figure 3d show that mostly the vibrating atoms within each mode contribute to the polarized Raman dipole, as

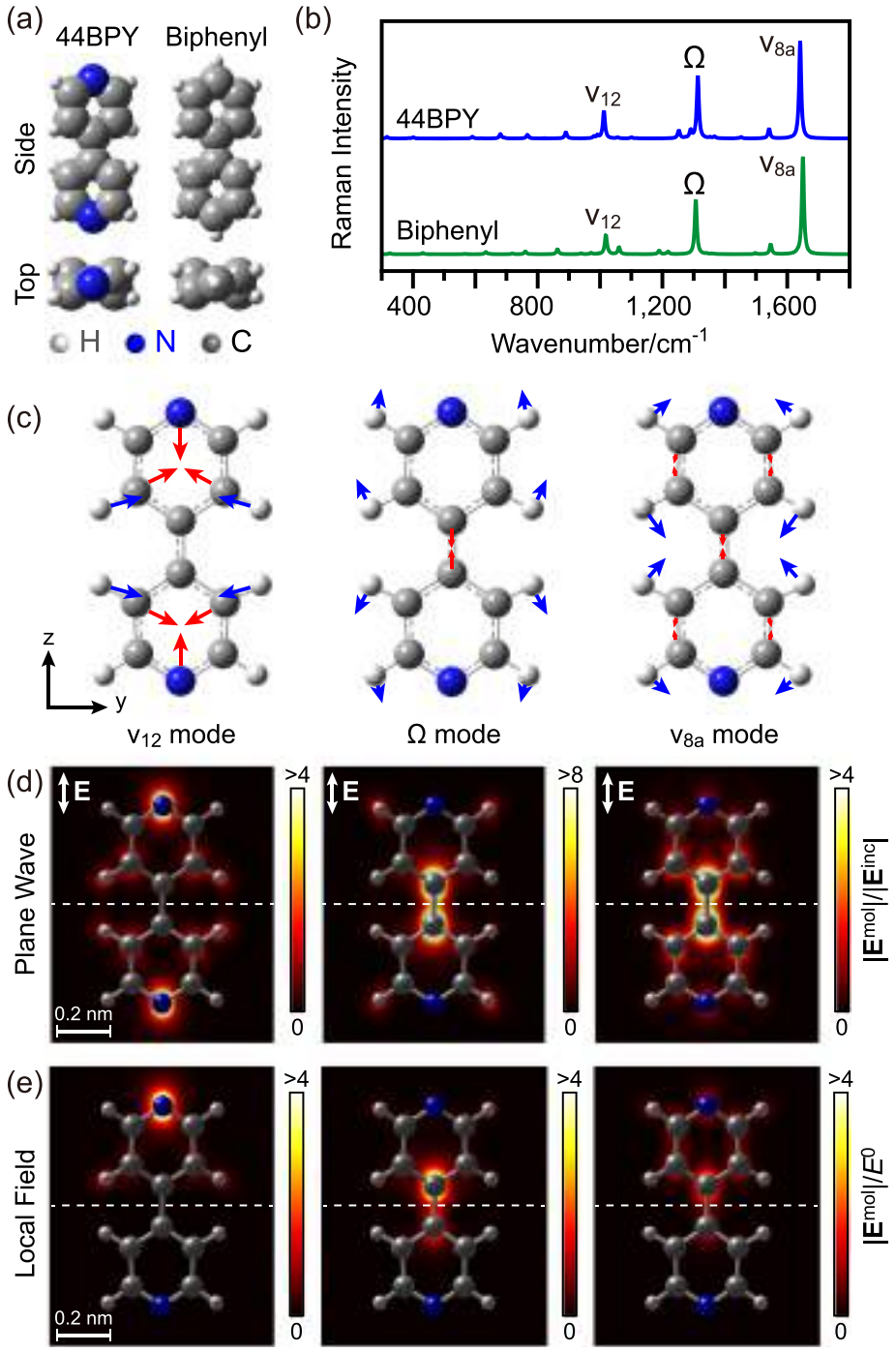

FIGURE 3 (a) Schematics of the chemical structures of 4,4′-bipyridine (44BPY) and biphenyl molecules from side and top views. (b) Calculated Raman spectra of 44BPY and biphenyl molecules within density functional theory (DFT) under homogeneous illumination. The three main vibrational peaks are labeled as v_{12}, Ω, and v_{8a} modes, respectively. (c) Vibrational motion of the three dominant vibrational modes (v_{12}, Ω, and v_{8a}) of the 44BPY molecule, associated with ring motions. The red and blue arrows highlight the characteristic motion of each mode. (d) Normalized electric field distribution within the two pyridine ring planes for the three different vibrational modes of the 44BPY molecule polarized by a plane wave polarized along the *z*-direction, as indicated by white arrows. The dashed lines indicate that the two pyridine ring planes are not coplanar. (e) Electric field distributions for the same modes as in (d), in response to a localized field characterized by a three-dimensional Gaussian profile with central polarization and full width at half maximum of 0.2 nm, centered 0.5 nm away from the center of the molecule along the *z*-axis. The maximum magnitude of this Gaussian-like local field at the original point is set to be E^0

observed in the corresponding induced Raman electric field. This introduces a way to distinguish different vibrational modes by specifying the corresponding local responses from each atom. Furthermore, this effect of the local induced dipole could be more efficiently produced by a local electric field source and thus would enable single-molecule imaging in real space. The vibrational modes of the biphenyl molecule and the corresponding electric field distributions can be found in the Supplementary Information. However, if the incident electric field is not a plane wave but an extremely localized field, the molecular response is different, as shown in Figure 3e. In this case, the field distribution of the incident local field is considered to adopt an ad-hoc Gaussian function in the three dimensions, of 0.2 nm full width at half maximum, and located 0.5 nm away from the center of the 44BPY molecule laterally (along the *y*-axis). Compared to the homogeneous illumination, this extreme case of localized illumination makes each atom to experience a different field intensity, as observed in Figure 3e, resulting in a very different total molecular polarization. This effect will determine the final activation or not of a

vibrational mode in the Raman spectrum, as we will see in the next section. The Gaussian-like local field used here has been adopted in order to show the main features of the activation of atoms related to each particular mode in an academic way. In the next section, we will detail this effect in the Raman spectrum, as identified in the realistic case of a molecule located in the local field of a picocavity generated by the atoms of a cluster, mimicking a tip.

3.3 | TERS of a single molecule in a picocavity

3.3.1 | Inhomogeneous field-enhanced Raman spectroscopy

Similar to the effect produced by an extremely localized gaussian source of light shown in the previous section, the apex of a metallic nanocluster mimicking the atomic protrusions at the end of a tip can equally produce an extremely confined local electric field distribution to probe a molecule. This strongly inhomogeneous field will make each atom in the molecule to experience a different electric field intensity, that is, a different value of $\mathbf{E}^{\mathrm{loc}}(\mathbf{r}_n)$ for each of its atoms (Equation 9), as visually shown on the left panels of Figure 4a–d. The atomistic molecular Raman dipole moment $\mathbf{p}^{\mathrm{Raman}}_{n,k}$ induced by this inhomogeneous near field can be calculated following the procedure described in Section 2.3 and in the Supporting Information. These atomistic Raman dipoles act as induced light sources whose electric field at the ith atom of the nanocluster can be expressed in terms of the Green's function as

$$\begin{aligned}\mathbf{E}^{\mathrm{Raman}}_{i,k} &= \sum_{n=1}^{M} \overleftrightarrow{\mathrm{G}}_k(\mathbf{r}_i,\mathbf{r}_n)\mathbf{p}^{\mathrm{Raman}}_{n,k} \\ &= \sum_{n=1}^{M} \overleftrightarrow{\mathrm{G}}_{in,k}\alpha^{(n)}_k \sum_{i'=1}^{N} \overleftrightarrow{\mathrm{G}}_{ni',k} \sum_{j'=1}^{N} \mathbf{A}^{-1}_{i'j'}\mathbf{E}^{\mathrm{inc}}_{j'}.\end{aligned} \tag{14}$$

This electric field thus further polarizes the atoms in the nanocluster, resulting in an enhanced Raman emission, which can be described following Equation (2) as

$$\sum_{j=1}^{N} \mathbf{A}_{ij}\cdot\mathbf{p}^{(k)}_j = \mathbf{E}^{\mathrm{Raman}}_{i,k}. \tag{15}$$

And hence, the nanocluster-enhanced Raman scattering cross section of the molecule can be obtained:

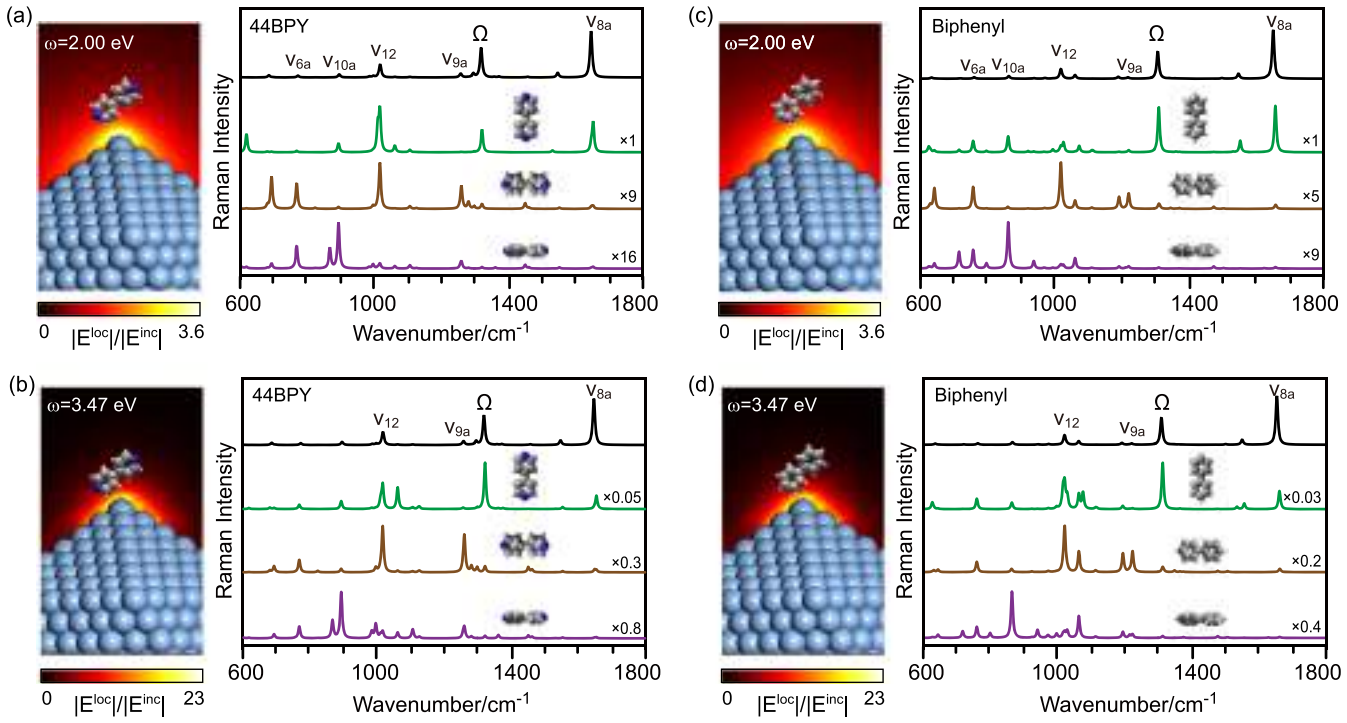

FIGURE 4 (a) Left: schematic of a 4,4′-bipyridine (44BPY) molecule located on top of a Ag_{1415} nanocluster at a distance of 0.5 nm under incident electromagnetic field with frequency $\omega = 2.00$ eV. Right: calculated Raman spectra of single 44BPY molecule with different orientations: upright standing (green spectrum), lying (brown spectrum), and flat lying (purple spectrum). The Raman spectrum of a 44BPY molecule in free space is also shown in black for reference. (b) Schematic (left) and calculated Raman spectra (right) of a 44BPY molecule at a distance of 0.5 nm from the apex of the nanocluster at a frequency $\omega = 3.47$ eV for the same orientations as in (a). (c) and (d) Same as in (a) and (b) for a biphenyl molecule

$$\frac{d\sigma_k^{\text{Raman}}}{d\Omega} = \frac{\omega_k^4}{16\pi^2\varepsilon_0^3 c^4}\left|\sum_{j=1}^{N}\mathbf{p}_j^{(k)}\right|^2. \quad (16)$$

The expression above includes the information of the Raman polarizability of the molecule via the atomistic dipoles of the cluster p_j^k. In this way, the Raman spectra under inhomogenous illumination can be calculated.

We apply this methodology to show how the effect of extreme field localization at the apex of a metallic tip results in a dramatic change of the Raman spectrum, often referred to as Raman selection rules breaking. We first consider the case of a single 44BPY molecule located on top of the apex of a Ag_{1415} nanocluster at a distance of 0.5 nm under off-resonance illumination (ω = 2.0 eV). The Raman spectrum for homogeneous illumination is displayed as a reference with a black line on top of the right panel of Figure 4a, as directly calculated from the DFT. However, when the molecule is located in the proximity of the apex at a distance of 0.5 nm from the apex, but its relative orientation changes (see insets for the relative orientations of the molecule in Figure 4a); dramatic changes in the Raman spectra occur. In addition to the three main vibrational modes, new modes emerge in the spectrum (see green, brown, and purple lines in the spectra of Figure 4a). The emergence of these new modes is a direct consequence of the inhomogeneous local field distribution. Similar results can be observed for the biphenyl molecule with the same orientation (spectra in Figure 4c).

The influence on the selection rules is more pronounced if the incident field is in resonance with the nanoresonator, and thus, more localized field is produced at the molecule. In Figure 4b,d, we consider the 44BPY and biphenyl molecule to be at a distance d = 0.5 nm under a incident electromagnetic field in resonance with the plasmonic cluster. The spectral features of the Raman intensities are further influenced in this case: by comparing the corresponding Raman intensities for the same molecular orientation in Figure 4a,b, it can be found that although the Raman peaks are generally enhanced, the relative intensities change differently. For the upright-standing orientation (green lines), the top N(C) and neighboring C atoms experience more intense electric field than other atoms for this particular configuration, resulting in an enhancement of the corresponding modes. For the

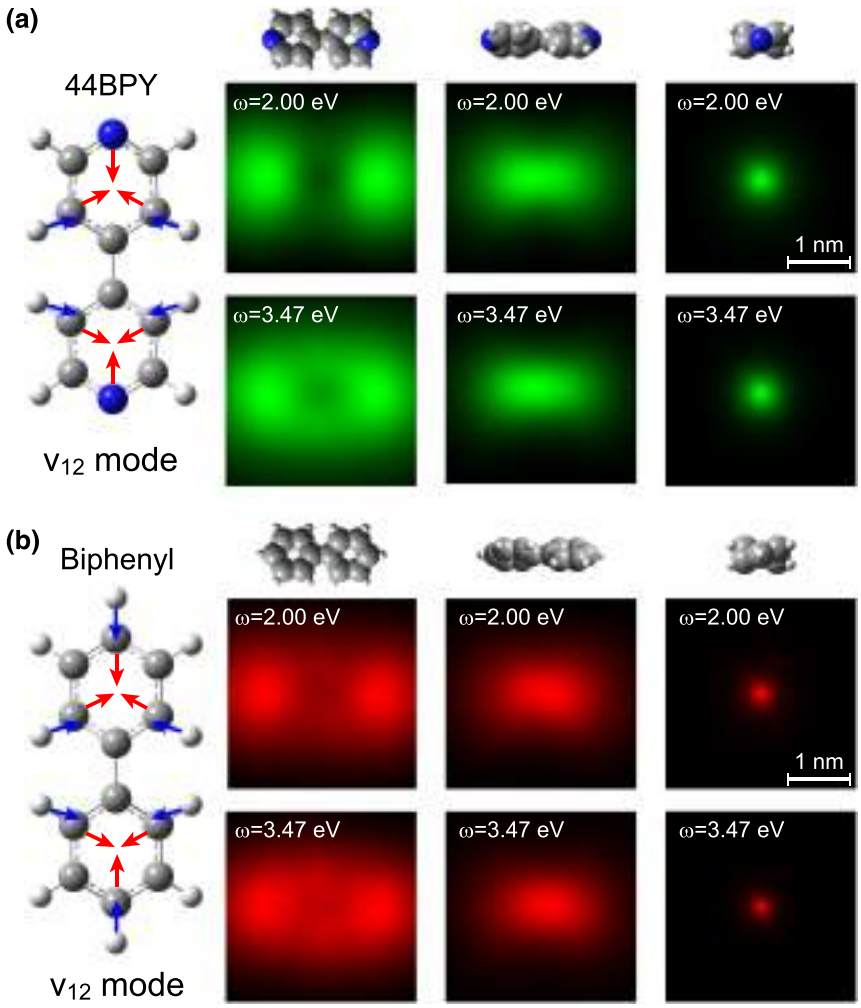

FIGURE 5 (a) Real-space mapping images of a single 4,4′-bipyridine (44BPY) molecule with different orientations as shown on the top of the mapping results. The schematics of the vibrational mode ν_{12} of the 44BPY molecule selected for the Raman mapping calculation is shown. The center of the molecule is located in the *xy*-plane 0.5 nm away from the apex of the nanocluster, although the orientation of molecule is rotated differently according to the molecular center. (b) Same mapping images for the biphenyl molecule

flat-lying and latericumbent-lying configurations (brown and purple lines in Figure 4b), the atomistic Raman spectrum is quite similar to the nonresonance illumination condition in Figure 4a, because for those particular configurations, all the atoms are located in a region of electric field with nearly homogeneous intensity distribution. This also coincides with the spectral features observed in experiments for the 44BPY molecule in a relatively homogeneous field.[65]

3.3.2 | Scanning Raman picoscopy

The extreme localization of the local field in the proximity of a tip apex at the atomic scale can serve for real-space imaging purposes when scanned over the molecule. To show this capability, we perform a simulation of the spatial distribution of the Raman peak intensity of the ν_{12} mode of the 44BPY molecule, as it is always present for all orientations. The ν_{12} mode is related to the breathing mode of the pyridyl rings; therefore, as shown in Figure 5a, the mapping of the mode at different molecular orientations and at different distances from the tip shows different patterns. For the flat-lying 44BPY molecule, the spatial Raman map under off-resonance illumination at a separation of 0.5 nm reveals a "dumbbell" feature, which coincides with the chemical structure of the 44BPY molecule. For the latericumbent-lying and flat-lying configurations, the images change according to the geometries of the single molecule. If the frequency of the incident electric field is resonant with the nanocluster, the corresponding Raman images are shrunk because of a tighter confinement of the local field. The spatial mapping of the biphenyl molecule (Figure 5b) shows similar features as the 44BPY molecule, except for the upright-standing configuration that provides more confined images because of the substitution of the N atoms into C and H atoms. This makes the biphenyl molecule slightly longer and thus closer to the apex of the nanocluster. These images clearly show the capability of a tip with atomic-scale features to map the Raman modes of a single molecule with atomic-scale resolution.

Finally, we address the issue of distinguishability of molecular species in the atomic-scale Raman maps.

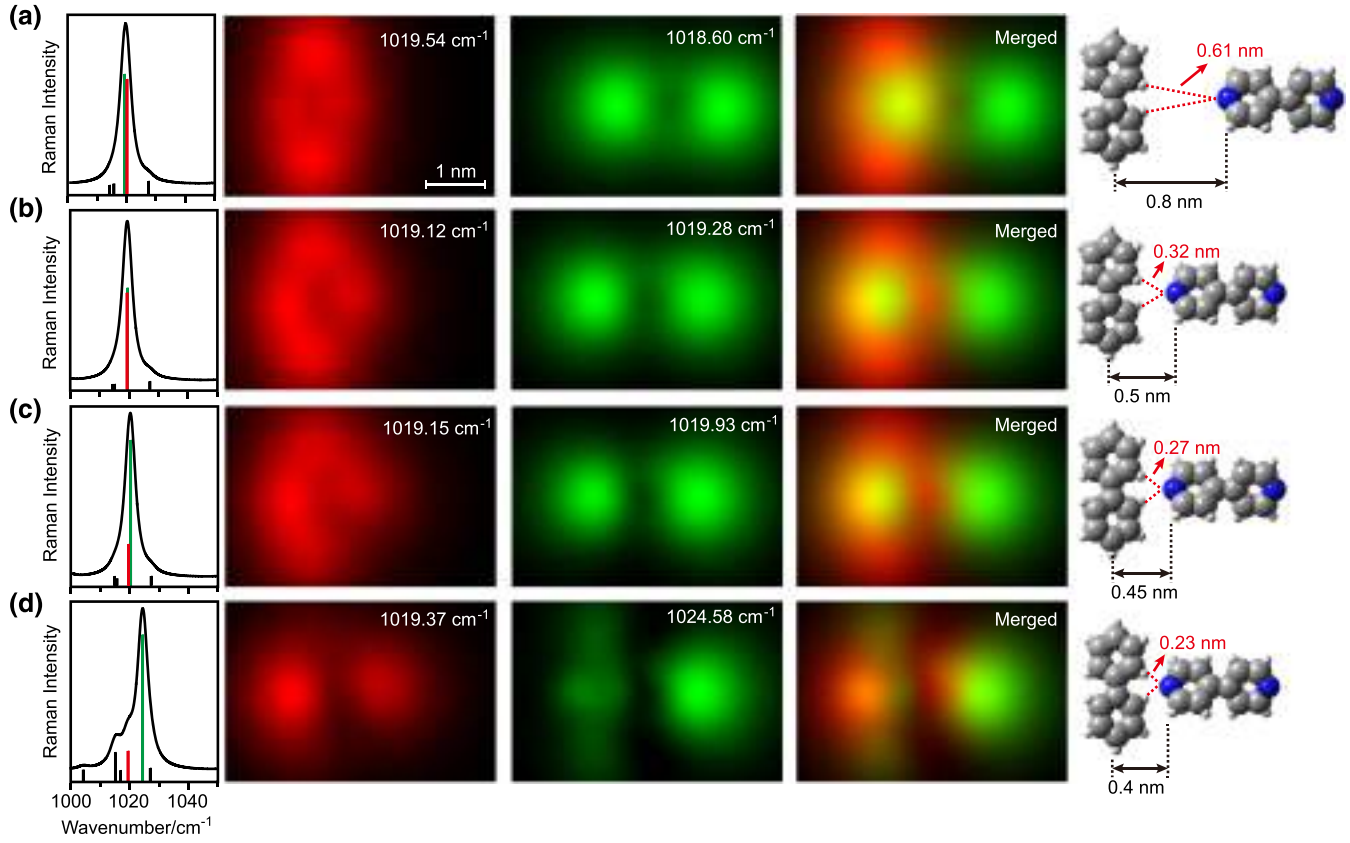

FIGURE 6 Real-space Raman mapping of two adjacent molecules (4,4′-bipyridine [44BPY] and biphenyl) for configurations with different separation distances, as described in the panels of the right-hand side: (a) 0.8, (b) 0.5, (c) 0.45, and (d) 0.4 nm with the N–H "bond" lengths labeled in red. The corresponding Raman spectra are shown on the left panels for each configuration as obtained from DFT calculations. The corresponding vibrational modes are displayed with red and green lines. The corresponding Raman maps for the the labeled peaks (second column for red lines and third column for green lines) and the merged images (fourth column) are shown

Because of the similarity of some molecules, such as 44BPY and biphenyl, it is usually hard to distinguish them from the Raman spectra, especially when they are mixed up together. However, with the aid of the ultra-high resolution provided by the local plasmonic fields, different molecules can be identified in real space from the spatial maps of the modes, as demonstrated in Figure 6. If the 44BPY and biphenyl molecules are separated far enough (e.g., 0.8 nm from each other as in Figure 6a), the spatial maps of the ν_{12} mode of both biphenyl and 44BPY molecules are similar but rotated by 90°, as shown in Figure 6. As the distance between the two molecules is reduced (0.5 and 0.45 nm, for instance), the Raman peak of the ν_{12} mode is still degenerated for both molecules; however, the spatial map of the modes exhibits asymmetric features. This effect is more pronounced as the 44BPY molecule approaches closer to the biphenyl molecule, as observed in Figure 6b–d. If the distance between two molecules is close enough (0.4 nm), they cannot be distinguished as two isolated entities in the map because the vibrations are no longer confined into one single molecule because of the strong interaction. If we consider that the distance between the N atom in 44BPY and the neighboring H atoms can be as small as 0.23 nm, it is likely to speculate that a hydrogen bond might be formed; that is, the two molecules get linked together and vibrate as a whole. The strong interaction between two molecules also results in the split of the Raman peaks, indicating that at such close interaction distance, the 44BPY and biphenyl molecules cannot be regarded as individual molecules anymore. The study of these effects shows the enormous potential of Raman picoscopy as a tool to formally distinguish different molecular species and their mutual interactions.

4 | CONCLUSIONS

We introduced a general treatment to calculate inhomogeneous field-enhanced Raman spectra from single molecules within a simplified calculation procedure. The Raman signal from molecules subjected to extremely localized plasmonic fields such as those produced at the atomic protrusions of scanning tips (picocavities) can be theoretically obtained within this approach. Furthermore, the calculation of the Raman signal when the picocavity-on-a-tip scans the molecule allows for reproducing and interpreting chemical maps of single molecules, as obtained in SRP. Within the method presented here, the Raman intensity of a vibrational mode can be calculated by adding up the contribution from the atomistic Raman dipoles associated with each atom of the molecule. The effect of the inhomogenous field on the Raman dipole, and thus on the Raman signal, is accounted for by conveniently weighting each calculated atomistic Raman dipole by the value of the local field at the corresponding atomic position. We applied this methodology to the case of an atomic-scale apex at the tip of a silver cluster probing 4,4′-BPY and biphenyl molecules. The enhanced Raman spectra were found to be sensitive to the orientation of the single molecules and to the distance between the single molecule and the apex of the tip, mainly due to the localization of the local fields at the atomic scale. This sensitivity can be exploited to perform spatial chemical mapping of single molecules with intramolecular resolution and to distinguish two adjacent similar molecules in real space. The methodology proposed here proves the importance of fully accounting for the atomistic features in plasmon-enhanced Raman scattering processes, which turns to be crucial to interpret single-molecule Raman mapping, as well as to exploit structural chemical information and reactivity of single molecules at the atomic scale.

ACKNOWLEDGEMENTS

The authors declare no competing financial interest. The authors thank Ruben Esteban for useful discussions. J. A. acknowledges projects IT1164-19 and KK-2019/00101 from the Government of the Basque Country and project PID2019-107432GB-I00 from the Spanish Ministry of Science and Innovation. Y. Z. acknowledges the National Natural Science Foundation of China (21804125), and Z. C. D. acknowledges the Chinese Academy of Science, the National Key R&D Program of China, and Anhui Initiative in Quantum Information Technologies.

ORCID

Zhen-Chao Dong https://orcid.org/0000-0002-4596-6269

Javier Aizpurua https://orcid.org/0000-0002-1444-7589

REFERENCES

[1] J. Wessel, *J. Opt. Soc. Am. B* **1985**, *2*(9), 1538.
[2] M. S. Anderson, *Appl. Phys. Lett.* **2000**, *76*, 3130.
[3] N. Hayazawa, Y. Inouye, Z. Sekkat, S. Kawata, *Opt. Commun.* **2000**, *183*(1-4), 333.
[4] B. Pettinger, G. Picardi, R. Schuster, G. Ertl, *Electrochemistry* **2000**, *68*, 942.
[5] R. M. Stöckle, Y. D. Suh, V. Deckert, R. Zenobi, *Chem. Phys. Lett.* **2000**, *318*(1-3), 131.
[6] A. Hartschuh, E. J. Sánchez, X. S. Xie, L. Novotny, *Phys. Rev. Lett.* **2003**, *90*(9), 95503.
[7] N. Anderson, A. Hartschuh, S. Cronin, L. Novotny, *J. Am. Chem. Soc.* **2005**, *127*(8), 2533.
[8] C. C. Neacsu, J. Dreyer, N. Behr, M. B. Raschke, *Phys. Rev. B* **2006**, *73*, 193406.
[9] J. Steidtner, B. Pettinger, *Phys. Rev. Lett.* **2008**, *100*, 236101.

[10] T. Yano, P. Verma, Y. Saito, T. Ichimura, S. Kawata, *Nat. Photonics* **2009**, *3*(8), 473.

[11] B. Pettinger, P. Schambach, C. J. Villagómez, N. Scott, *Annu. Rev. Phys. Chem.* **2012**, *63*, 379.

[12] Z. He, Z. Han, M. Kizer, R. J. Linhardt, X. Wang, A. M. Sinyukov, J. Wang, V. Deckert, A. V. Sokolov, J. Hu, M. O. Scully, *J. Am. Chem. Soc.* **2019**, *141*(2), 753.

[13] R. Kato, S. Igarashi, T. Umakoshi, P. Verma, *ACS Appl. Nano Mater.* **2020**, *3*(6), 6001.

[14] W. Zhang, B. S. Yeo, T. Schmid, R. Zenobi, *J. Phys. Chem. C* **2007**, *111*(4), 1733.

[15] M. D. Sonntag, J. M. Klingsporn, L. K. Garibay, J. M. Roberts, J. A. Dieringer, T. Seideman, K. A. Scheidt, L. Jensen, G. C. Schatz, R. P. Van Duyne, *J. Phys. Chem. C* **2011**, *116* (1), 478.

[16] R. Zhang, Y. Zhang, Z. C. Dong, S. Jiang, C. Zhang, L. G. Chen, L. Zhang, Y. Liao, J. Aizpurua, Y. Luo, J. L. Yang, J. G. Hou, *Nature* **2013**, *498*, 82.

[17] H. Xu, J. Aizpurua, M. Käll, P. Apell, *Phys. Rev. E* **2000**, *62*(3), 4318.

[18] M. Moskovits, *Rev. Mod. Phys.* **1985**, *57*(3), 783.

[19] E. C. Le Ru, P. G. Etchegoin, *Chem. Phys. Lett.* **2006**, *423* (1-3), 63.

[20] P. Alonso-González, P. Albella, M. Schnell, J. Chen, F. Huth, A. García-Etxarri, F. Casanova, F. Golmar, L. Arzubiaga, L. E. Hueso, J. Aizpurua, R. Hillenbrand, *Nat. Commun.* **2012**, *3*, 684.

[21] A. Otto, *J. Raman Spectrosc.* **2005**, *36*(6-7), 497.

[22] P. Roelli, C. Galland, N. Piro, T. J. Kippenberg, *Nat. Nanotechnol.* **2016**, *11*(2), 164.

[23] M. K. Schmidt, R. Esteban, A. González-Tudela, G. Giedke, J. Aizpurua, *ACS Nano* **2016**, *10*(6), 6291.

[24] M. K. Schmidt, R. Esteban, F. Benz, J. J. Baumberg, J. Aizpurua, *Faraday Discuss.* **2017**, *205*, 31.

[25] F. Benz, M. K. Schmidt, A. Dreismann, R. Chikkaraddy, Y. Zhang, A. Demetriadou, C. Carnegie, H. Ohadi, B. de Nijs, R. Esteban, J. Aizpurua, J. J. Baumberg, *Science* **2016**, *354*, 726.

[26] Z. Yang, J. Aizpurua, H. Xu, *J. Raman Spectrosc.* **2009**, *40*, 1343.

[27] S. Trautmann, J. Aizpurua, I. Götz, A. Undisz, J. Dellith, H. Schneidewind, M. Rettenmayr, V. Deckert, *Nanoscale* **2017**, *9*(1), 391.

[28] M. Barbry, P. Koval, F. Marchesin, R. Esteban, A. G. Borisov, J. Aizpurua, D. Sánchez-Portal, *Nano Lett.* **2015**, *15*(5), 3410.

[29] M. Micic, N. Klymyshyn, Y. D. Suh, H. P. Lu, *J. Phys. Chem. B* **2003**, *107*(7), 1574.

[30] M. Rahaman, A. G. Milekhin, A. Mukherjee, E. E. Rodyakina, A. V. Latyshev, V. M. Dzhagan, D. R. T. Zahn, *Faraday Discuss.* **2019**, *214*, 309.

[31] C. Oubre, P. Nordlander, *J. Phys. Chem. B* **2004**, *108*, 17740.

[32] Z. Yang, Q. Li, F Ruan, Z. Li, B. Ren, H. Xu, Z. Tian, *Chin. Sci. Bull.* **2010**, *55*, 2635.

[33] F. J. G. De Abajo, J. Aizpurua, *Phys. Rev. B* **1997**, *56*, 15873.

[34] J. Aizpurua, S. P. Apell, R. Berndt, *Phys. Rev. B* **2000**, *62*, 2065.

[35] C. Huber, A. Trügler, U. Hohenester, Y. Prior, W. Kautek, *Phys. Chem. Chem. Phys.* **2013**, *16*, 2289.

[36] M. Yang, M. S. Mattei, C. R. Cherqui, X. Chen, R. P. Van Duyne, G. C. Schatz, *Nano Lett.* **2019**, *19*(10), 7309.

[37] J. Zuloaga, E. Prodan, P. Nordlander, *Nano Lett.* **2009**, *9* (2), 887.

[38] D. C. Marinica, A. K. Kazansky, P. Nordlander, J. Aizpurua, A. G. Borisov, *Nano Lett.* **2012**, *12*(3), 1333.

[39] A. Varas, P. García-González, J. Feist, F. J. García-Vidal, A. Rubio, *Nanophotonics* **2016**, *5*(3), 409.

[40] E. Selenius, S. Malola, H. Häkkinen, *J. Phys. Chem. C* **2017**, *121*, 27036.

[41] M. Z. Herrera, A. K. Kazansky, J. Aizpurua, A. G. Borisov, *Phys. Rev. B* **2017**, *95*, 245413.

[42] L. Jensen, C. M. Aikens, G. C. Schatz, *Chem. Soc. Rev.* **2008**, *37*, 1061.

[43] L. L. Jensen, L. Jensen, *J. Phys. Chem. C* **2009**, *113*, 15182.

[44] X. Chen, J. E. Moore, M. Zekarias, L. Jensen, *Nat. Commun.* **2015**, *6*, 8921.

[45] X. Chen, P. Liu, Z. Hu, L. Jensen, *Nat. Commun.* **2019**, *10*(1), 2567.

[46] S. Jiang, Y. Zhang, R. Zhang, C. Hu, M. Liao, Y. Luo, J. Yang, Z. Dong, J. G. Hou, *Nat. Nanotechnol.* **2015**, *10*(10), 865.

[47] J. Lee, T. Crampton K., N. Tallarida, V. Ara Apkarian, *Nature* **2019**, *568*, 78.

[48] Y. Zhang, B. Yang, A. Ghafoor, Y. Zhang, Y. F. Zhang, R. P. Wang, J. L. Yang, Y. Luo, Z. C. Dong, J. G. Hou, *Natl. Sci. Rev.* **2019**, *6*(6), 1169.

[49] J. J. Baumberg, J. Aizpurua, M. H. Mikkelsen, D. R. Smith, *Nat. Mater.* **2019**, *18*, 668.

[50] H. H. Shin, G. J. Yeon, H. K. Choi, S. M. Park, K. S. Lee, Z. H. Kim, *Nano Lett.* **2018**, *18*(1), 262. PMID: 29206468.

[51] C. Carnegie, J. Griffiths, B. de Nijs, C. Readman, R. Chikkaraddy, W. M. Deacon, Y. Zhang, I. Szabó, E. Rosta, J. Aizpurua, J. J. Baumberg, *J. Phys. Chem. Lett.* **2018**, *9*, 7146.

[52] M. Urbieta, M. Barbry, Y. Zhang, P. Koval, D. Sánchez-Portal, N. Zabala, J. Aizpurua, *ACS Nano* **2018**, *12*(1), 585.

[53] P. Liu, D. V. Chulhai, L. Jensen, *ACS nano* **2017**, *11*(5), 5094.

[54] S. Duan, G. Tian, Y. Ji, J. Shao, Z. Dong, Y. Luo, *J. Am. Chem. Soc.* **2015**, *137*, 9515.

[55] E. M. Purcell, C. R. Pennypacker, *Astrophys. J.* **1973**, *186*, 705.

[56] M. J. Frisch, Gaussian 09 Revision A.01, Gaussian Inc. Wallingford CT, **2009**.

[57] P. B. Johnson, R. W. Christy, *Phys. Rev. B* **1972**, *6*, 4370.

[58] P. Zhang, J. Feist, A. Rubio, P. García-González, F. J. García-Vidal, *Phys. Rev. B* **2014**, *90*, 161407.

[59] B. Doppagne, M. C. Chong, E. Lorchat, S. Berciaud, M. Romeo, H. Bulou, A. Boeglin, F. Scheurer, G. Schull, *Phys. Rev. Lett.* **2017**, *118*, 127401.

[60] B. Doppagne, T. Neuman, R. Soria-Martinez, L. E. P. López, H. Bulou, M. Romeo, S. Berciaud, F. Scheurer, J. Aizpurua, G. Schull, *Nat. Nanotechnol.* **2020**, *15*(3), 207.

[61] R. B. Jaculbia, H. Imada, K. Miwa, T. Iwasa, M. Takenaka, B. Yang, E. Kazuma, N. Hayazawa, T. Taketsugu, Y. Kim, *Nat. Nanotechnol.* **2020**, *15*(2), 105.

[62] B. Yang, G. Chen, A. Ghafoor, Y. Zhang, Y. Zhang, Y. Zhang, Y. Luo, J. Yang, V. Sandoghdar, J. Aizpurua, Z. Dong, J. G. Hou, *Nat. Photonics* **2020**, 1. https://doi.org/10.1038/s41566-020-0677-y

[63] G. Varsányi, L. Láng, *Assignments for Vibrational Spectra of Seven Hundred Benzene Derivatives*, Wiley, New York **1974**.

[64] L. Ould-Moussa, O. Poizat, M. Castellá-Ventura, G. Buntinx, E. Kassab, *J. Phys. Chem.* **1996**, *100*(6), 2072.

[65] Y. Zhang, R. Zhang, S. Jiang, Y. Zhang, Z. C. Dong, *ChemPhysChem* **2019**, *20*(1), 37.

SUPPORTING INFORMATION

Additional supporting information may be found online in the Supporting Information section at the end of this article.

How to cite this article: Zhang Y, Dong Z-C, Aizpurua J. Theoretical treatment of single-molecule scanning Raman picoscopy in strongly inhomogeneous near fields. *J Raman Spectrosc.* 2021;52:296–309. https://doi.org/10.1002/jrs.5991